

# Practical RGB Measurement of Fluorescence and Blood Distributions in Skin

Emilie Nogué; Imperial College London and Lumirithmic Ltd; London, United Kingdom

Arvin Lin; Imperial College London and Lumirithmic Ltd; London, United Kingdom

Xiaohui Li; Imperial College London and Lumirithmic Ltd; London, United Kingdom

Giuseppe Claudio Guarnera; University of York and Lumirithmic Ltd; York, United Kingdom

Abhijeet Ghosh; Imperial College London and Lumirithmic Ltd; London, United Kingdom

## Abstract

Biophysical skin appearance modeling has previously focused on spectral absorption and scattering due to chromophores in various skin layers. In this work, we extend recent practical skin appearance measurement methods employing RGB illumination to provide a novel estimate of skin fluorescence, as well as direct measurements of two parameters related to blood distribution in skin – blood volume fraction, and blood oxygenation. The proposed method involves the acquisition of RGB facial skin reflectance responses under RGB illumination produced by regular desktop LCD screens. Unlike previous works that have employed hyperspectral imaging for this purpose, we demonstrate successful isolation of elastin-related fluorescence, as well as blood distributions in capillaries and veins using our practical RGB imaging procedure.

## Introduction

Modeling and measuring facial skin appearance have received significant attention in computer graphics and vision due to their crucial role in rendering realistic digital humans. Skin appearance provides valuable insights into an individual’s health and lifestyle [4, 22, 26]. This has led to extensive studies of skin optical properties in tissue optics and dermatology. Researchers have developed biophysically based skin appearance models inspired by tissue optics literature. These models simulate skin reflectance response and various physiological effects, including tanning, blushing/blood flow, and skin aging [8, 9, 20, 18].

However, these studies mainly focus on modeling skin reflectance based on light absorption and scattering by chromophores in skin layers, without considering skin fluorescence. Auto-fluorescence is a natural skin function. Beyond light reflection, certain skin components - namely fluorophores - absorb high-energy photons and re-emit them as lower-energy light at longer wavelengths. This signal is exploited in the medical domain for the assessment of skin health and the detection of diseases [22, 13]. These methods require complex optical equipment, including UV response imaging, and are not easily scalable to full facial measurements. Measuring the skin fluorescence can enhance scattering simulations, improve albedo prediction, and help infer mechanical properties for skin deformation modeling.

In this work, we present a novel method for the practical measurement of skin elastin fluorescence using RGB imaging, which allows us to separate spectral skin reflectance from fluorescence responses due to fluorophores. Our approach uses a data-driven re-radiation matrix (also referred to as the Donaldson

matrix [7]) to simulate the facial elastin fluorescence albedo response to specific excitation-emission wavelength combinations. Our method leverages spectral information without hyperspectral equipment and identifies standalone entities of skin.

Additionally, our RGB measurements directly yield maps of blood volume fraction and blood oxygen rate with minimal post-processing. Blood volume fraction, which indicates the proportion of blood volume within a tissue in both the dermis and epidermis, is typically referred to as redness in dermatological skin analysis [27]. In medical imaging, this quantity is usually estimated by magnetic resonance imaging (MRI) or computed tomography (CT) scans. The Antera device used in Gitlina et al. [15] estimates a single redness map that is then mapped to two hemoglobin parameters. Our blood volume fraction map achieves comparable quality using RGB illumination rather than the dense set of multispectral measurements required by the previous work.

We also measure the blood oxygen rate, which tracks the transport of oxygen by hemoglobin throughout the skin. Together with blood volume fraction, this provides a comprehensive map of blood flow and tissue oxygenation across the face, neck, and ears. Unlike most previous studies, our method directly isolates both fluorescence and blood distributions using practical RGB measurements, *without* relying on the assumption of a specific biophysical skin model.

## Related Work

In this section, we give a brief overview of the recent studies most related to our measurements. For an extensive overview of skin appearance measurement and modelling, please refer to surveys on skin [17], facial appearance acquisition [30, 21] and medical hyperspectral imaging [24].

## Medical Analysis of Skin Optical Properties

Skin is a complex organ made up of various components acting on multiple scales, producing a distinctive spectral signature. Measuring the optical properties of skin provides a wealth of information about the health of an individual. This has generated consistent interest in non-invasive, in-vivo skin measurements, which have the benefit of obtaining direct measurements without altering the skin tissue. Several key techniques have been developed, including diffuse reflectance spectroscopy [31], modulated imaging [5], and spectral imaging [6, 28]. Hyperspectral imaging [24] captures images across multiple wavelength bands. As a highly useful non-invasive tool, it provides numerous data points for analysis of optical skin properties.

This information is usually processed using skin and optical models, with the computation time increasing with the quantity of information. Closest to our work, Gevaux et al. [10] employ a hyperspectral camera setup to extract melanin, blood volume fraction, and oxygen rate with a skin-model-driven optimization. Later work [11] employs the same measurements but replaces the optimization with a neural network, reducing acquisition time from 5 hours to 2 seconds.

### **Biophysical Skin Measurement in Computer Graphics and Computer Vision**

Recent works have focused on both RGB and spectral measurements of skin, acquiring physiological maps of skin in order to better analyse, recreate and edit its appearance. Jensen et al. [19] developed a subsurface scattering model for translucent materials and a rapid imaging technique using a focused white beam to measure optical properties. Their approach efficiently simulates light diffusion and color bleeding in materials like skin, milk, and marble. Tsumura et al. [29] employed independent component analysis of images using UV-B irradiation and topical chemical application to retrieve melanin and hemoglobin maps for skin appearance editing based on physiological data. Donner et al. [9] developed detailed skin reflectance models using multispectral imaging of skin patches, while other studies focused on facial measurement with a color camera under uniform broadband illumination to estimate skin properties [20]. This data was used to estimate melanin and hemoglobin concentrations and the evolution of hemoglobin through facial expressions, following the protocol of [4], which employs controlled color imaging and spectral analysis to generate parametric maps of pigmentation and blood content. Gotardo et al. [16] proposed a multi-view setup using static illumination to capture dynamic facial skin properties.

Measurements have been performed using broadband illumination from a lightstage to estimate melanin and hemoglobin concentrations and drive a morphable model of skin appearance [2]. The work of Gitlina et al. [14] builds on this research to produce maps of four different chromophores from RGB images, using a skin model-based neural network and the combined use of broadband and narrowband LED illumination. Aliaga et al. [1] proposed a network to predict spectral skin reflectance in the visible and the near-infrared range from RGB measurements.

We demonstrate that our method can directly measure blood oxygen rate and blood volume fraction, providing a map that estimates two parameters previously studied: dermal and epidermal hemoglobin. Additionally, we capture a fluorescence signal induced by elastin. Unlike previous approaches, our method achieves these spectral measurements from an RGB setup without relying on an underlying biophysical skin appearance model.

### **Measurement Setup**

Our experimental setup follows the monitor-based system of Lattas et al. [23]. Illumination is provided by four 4K desktop LCD monitors (Asus 347 ProArt PA279CV) arranged in a half-circle around the subject, providing linearly polarized light for illumination. Using four large monitors ensures adequate coverage and spatially uniform illumination across the face of subjects.

These monitors create a nearly uniform half-hemispherical lighting, minimizing intensity variations. While we employ these specific LCD panels, any LCD illumination with a comparable,

known Spectral Power Distribution (SPD) could be employed interchangeably.

Images are captured using a Canon mirrorless camera (EOS M6 Mark II) positioned directly in front of the subject and a second camera facing the subject at a 45° angle. Both cameras are fitted with linear polarisers, cross-polarized w.r.t the monitors. This configuration enables specular-diffuse separation, following the approach in Ghosh et al. [12].

The SPD of the LCD panels, determined with a spectrometer (Sekonic SpectroMaster C700), is depicted by colored areas in Fig. 1. Additionally, the spectral sensitivity of the camera's RGB channels, measured with a monochromator, is shown as plotted lines in Fig. 1.

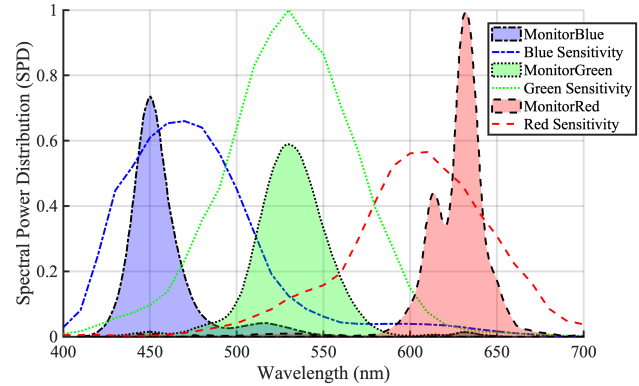


**Figure 1.** Spectral power distributions of the RGB illumination of the LCD panels as measured with a spectrometer (Sekonic SpectroMaster C700) and spectral sensitivity of the RGB cameras (Canon EOS M6 Mark II) used in this work.

HDR images of illuminated faces are captured at different exposures and under three distinct uniform illumination conditions: narrowband red, green, and blue, displayed on LCD panels, as illustrated in Fig. 2. These exposures are combined to extend the dynamic range of radiance values. To ensure consistency, images are aligned using optical flow to eliminate motion artifacts.

Color calibration is not required in our approach because we focus on capturing the normalized relative radiance across RGB bands, which HDR provides. The spectra of these bands are known and illustrated in Fig. 1. Unlike methods such as Gitlina et al. [14], which rely on skin model matching and therefore require accurate colorimetric data for perceptual metrics and radiometric calibration, our method measures scene radiance per RGB band. This inherently captures the spectral intensity information necessary for fluorescence and blood distribution measurements, eliminating the need for additional color calibration steps.

Isolating the diffuse response is particularly important as it provides valuable information about the optical properties and composition of scattering media such as biological tissues. Unlike specular reflectance which follows the law of reflection, diffuse reflectance typically involves multiple scattering events, creating an optical signature unique to a material.

In our work we leverage the fact that diffuse light penetrates deeper into skin layers, allowing for a non-invasive probing of subsurface skin composition and structures.

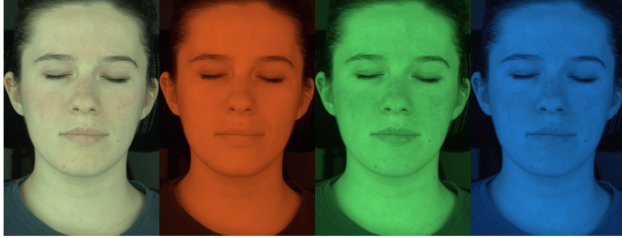


**Figure 2.** HDR images of a subject under red, green and blue illumination emitted by the LCD panels in our setup. These diffuse illuminations reveal skin components of different spectral sensitivities, penetrating different skin depths based on wavelength.

## Practical Fluorescence Measurement and Analysis

Elastin is a key structural protein in skin that provides elasticity and resilience [3]. Measuring elastin fluorescence and tracking its evolution over time can inform us on the health and integrity of the skin’s structure, indicating age-related processes and skin conditions. Additionally, elastin helps collagen, the main scatterer in skin, maintain its structural integrity.

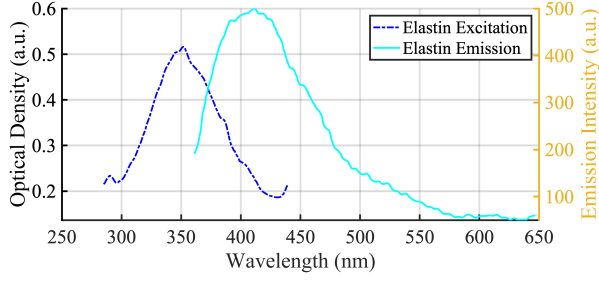


**Figure 3.** Excitation and emission spectrum of elastin protein in skin from Pu et al. [26]. The excitation spectrum covers the lowest wavelength of the visible spectrum which makes it an accessible skin fluorophores to measure without the use of potentially harmful UV lights.

In this work, we aim to isolate elastin fluorescence using a standard RGB camera under visible RGB illumination. By using a specific combination of LCD panel spectral power distribution (SPD) and camera sensitivity, we excite elastin fluorescence at wavelengths above 400 nm, on the tail end of the excitation, as shown in Fig. 3. This fluorescence appears in the green and blue channels of the camera, along with reflectance and absorption from other skin components. To distinguish elastin fluorescence from other signals, we leverage the fact that elastin absorbs UV and blue light and re-emits it at longer wavelengths. Specifically, when illuminated by the blue light from the LCD panel, elastin fluorescence generates a green signal in the camera’s green channel.

The green channel captured under blue light contains fluorescence, blue reflectance, and a small amount of green reflectance, as shown in Fig. 4. To isolate the fluorescence, we subtract both blue and green reflectance by scaling the blue channel (captured under blue light) and the green channel (captures under green light) according to their respective contributions to the overall signal. Reflection and absorption are proportional to the stimulation light and are scaled for accurate subtraction, while fluorescence,

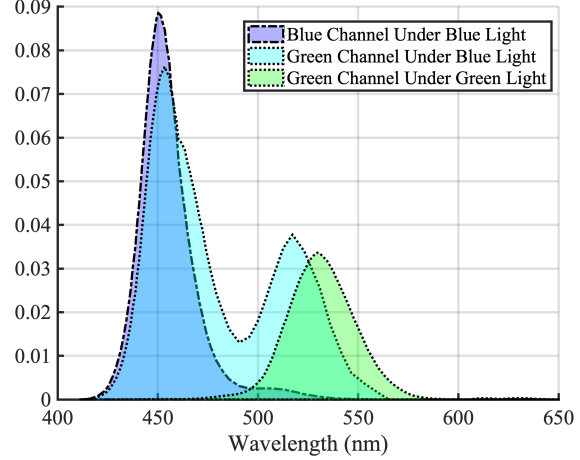


**Figure 4.** Plots of the different setup-specific spectral signals used to scale the green and blue images of Fig 2 in order to compute the quantity of elastin in skin depicted in Fig 5.



**Figure 5.** Facial skin elastin fluorescence maps simulated under a 365nm Dirac excitation. The emission is computed based on predicted elastin quantity per pixel and known elastin emission spectra.

due to its distinct excitation-emission process, remains isolated.

From these operations, we obtain a map of concentration of elastin in the skin. We compute the response of this concentration map to a UV illumination at 365nm as

$$F = \int_{\Omega} C(\lambda_o) Em(\lambda_o) \left( \int_{SPD} Ex(\lambda_i) I(\lambda_i) d\lambda_i \right) d\lambda_o. \quad (1)$$

Where  $C$  is the sensitivity of the camera sensor channel,  $Em$  is the emission spectrum of the considered fluorophore,  $\Omega$  is the domain of all possible emission wavelengths,  $Ex$  is the excitation spectrum of the considered fluorophore,  $SPD$  is the wavelength domain of the illumination and  $I$  is the intensity of the illumination at a specific wavelength. We chose 365 nm because it is the peak of elastin response in skin as per the Donaldson matrix of elastin computed with compiled data [26]. Fig. 5 is the result of such a computation for an illumination that is a Dirac peak at 365nm in the UV.

The elastin fluorescence signal in Fig. 5 demonstrates a correlation with skin thickness. Predominantly found in the dermis, elastin concentration varies with the thickness of the dermis layer across facial regions.

Effectively, areas with thicker skin such as the forehead, nose and cheeks show a stronger signal. Conversely, the eyelids, characterized by thinner skin, display a relatively weaker signal. Despite the lips theoretically having thinner layers, their abundance of elastin, crucial for elasticity, contributes to a strong signal. Results vary from one individual to another as depicted in Fig. 14. Factors like age and gender influence elastin content and overall skin thickness. Notably, individuals with higher melanin levels tend to display less fluorescence due to melanin absorption, which can directly impact elastin's absorption and emission spectra.

## Practical Measurement of Blood Volume Fraction and Oxygen Rate

### Computation of Blood Volume Fraction Map

In this section, we evaluate the proportion of blood in facial skin tissue. This quantity, often referred to as blood volume fraction, is key for understanding perfusion, oxygenation, and other hemodynamic parameters.

In this method we employ diffuse lighting to probe into skin layers, allowing us to analyze subsurface skin composition and structures non-invasively. Fig. 6 shows four distinct curves representing the green and blue camera channel responses under green and blue light. These curves, which are derived from the LCD screen spectral power density and camera sensitivity, help us understand how light interacts with skin. To isolate the blood volume fraction response of the skin, we subtract the skin's blue response under blue light from its response under green light. This subtraction isolates the signal in a narrow band around 450 nm, where hemoglobin absorption is prominent (see Fig. 7a).

However, this signal still includes green reflectance that was not eliminated by the initial subtraction. To address this, we compute a second image in Fig. 7b by subtracting of the green skin response under blue light from the same response under green light. As shown in Fig. 6, this subtraction aligns and eliminates the peaks of the green channel spectra, isolating the hemoglobin response around 450 nm. Although this results in a noisier signal, it provides a clearer indication of blood volume fraction.

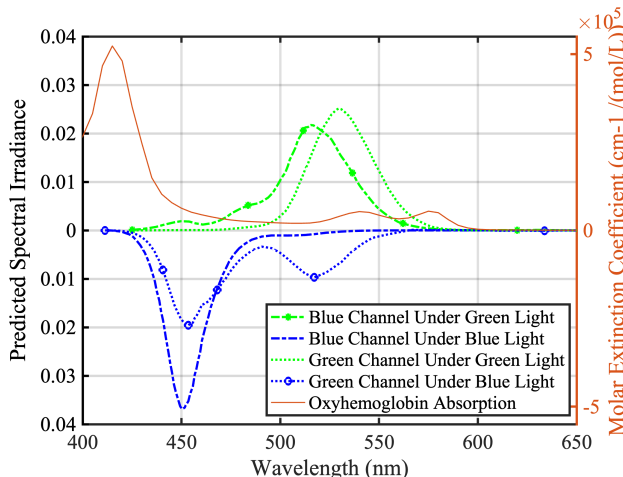


**Figure 6.** Green and blue camera channel spectral responses under green and blue light, derived from LCD screen spectral power density and camera sensitivity. We plot oxyhemoglobin absorption from compiled data [25].

We generate the initial blood volume map (left in Fig. 7). This method effectively isolates the hemoglobin response in the face and the map reveals blood vessels in areas such as the cheeks, ears, eyelids, and lips of the subject. The visibility of these vessels is influenced by skin thickness, with female subjects, typically having thinner skin layers, exhibiting higher visibility, as illustrated in additional results in Fig. 15.

A second map is computed by subtracting the green response under blue light (negative dotted blue in Fig. 6) from the response under green light (positive dotted green in Fig. 6). This map (Fig. 7b) provides a noisier but more pronounced measure of blood volume fraction.



**Figure 7.** Preliminary maps of blood volume fraction (left and center) and final results (right). The left image represents the subtraction of the blue skin response under blue light from that under green light, while the center image represents the subtraction of the green skin response under blue light from that under green light (Fig. 6). Blood volume fraction maps in skin, derived from the average of the first two blood maps, reveal a robust signal for capillaries in the eyelids, ears, and lips with improved signal-to-noise ratio compared to the initial blood maps.

Finally, we average the first two images in Fig. 7 to reduce noise and obtain images of the blood volume fraction in skin, mapping out the blood volume fraction in all upper layers of facial skin as seen in Fig. 7c.

In Fig. 7c, the depicted subject is a light-skinned female. The result map reveals heightened blood volume fractions in facial regions, including the cheeks, lips, and areas around the eyes, associated with the presence of capillaries and blood vessels. Result disparities among subjects are shown in Fig. 15. Notably, the maps demonstrate increased visibility in individuals with thinner skin [18], wherein capillaries and blood vessels are closer to the skin surface. Visibility is decreased in subjects with higher melanin rates as melanin absorption interferes directly with the capture of the signal.

### Computation of Oxygen Rate Maps

Oxygen in skin plays an important role in tissue health and wound healing. Oxygen levels in skin are influenced by external factors such as environment, UV exposure, pollution and temperature changes. Monitoring the oxygen rate in skin can yield important markers for skin health and metabolism. In this section, we aim to evaluate the oxygen rate in facial skin tissue.

Fig. 8 shows various signals crucial for estimating the oxygen rate map. These signals represent the detection of light by a camera sensor channel across different wavelengths under monochromatic LCD panel illumination. The red plot highlights two peaks in red light reflection detection, with one peak aligning precisely with the green reflection under green illumination.

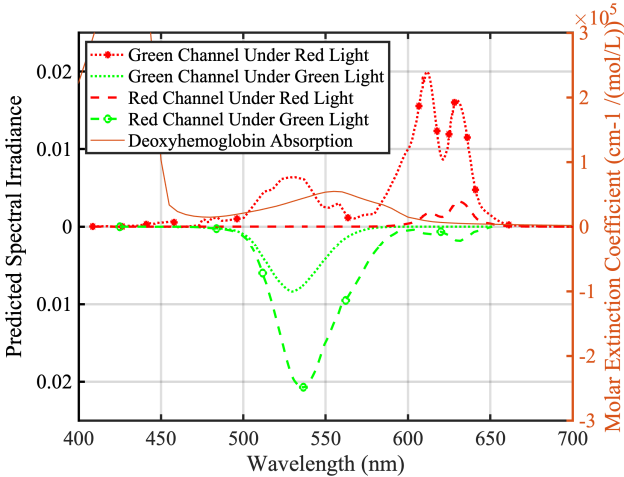


**Figure 8.** Curves in this plot represent signals crucial for oxygen rate mapping. The red curves display peaks of red light reflection (positive curves), coinciding with peaks of the green reflection (negative curve). We plot deoxyhemoglobin absorption from compiled data [25].

In Fig. 9a, we generate a first oxygen rate map by analyzing the skin's green response under red light, denoted by the positive, dotted red curve in Fig. 8. This response includes deoxyhemoglobin absorption, along with peaks for green and red reflectance. To isolate the deoxyhemoglobin absorption, we subtract the green response under green light from this signal. This subtraction removes the green reflectance peak and any absorption within the green bandwidth, as the green response under green light, shown in Fig. 8, precisely matches the green reflectance we want to eliminate.

Similar to the initial oxygen rate image in Fig. 9a, we construct a second map in Fig. 9b. This is achieved by examining the red response of the skin under red light, where the maximum reflectance is represented in positive dashed red in Fig. 8. We then subtract the red response of the skin under green light, illustrated in negative dashed green. In contrast to the left result in Fig. 9, this second method enhances the signal of oxygen rate. This approach enhances the oxygen rate signal and reveals veins containing deoxygenated blood, particularly visible on the temples and cheeks of the subject. However, this method also increases green light reflectance, which is noticeable in the resulting image.

In the final step, we reduce the noise level of the signal by averaging the first two images in Fig. 9 and obtain Fig. 9c. This process results in a clearer representation of the oxygen rate mapping in the skin, eliminating the reflectance observed in Fig. 9b. Additional results are presented in Fig. 16.

Notably, deoxygenated veins become more prominent, particularly in the neck of male light-skinned subjects. The oxygen rate is also more discernible, especially in individuals with lower concentrations of melanin as well as thinner skin layers, commonly observed in female subjects.

## Comparison

Our blood volume fraction map on the right in Fig. 10 represents what two separate hemoglobin parameters of a biophysical skin appearance model employed in Gitlina et al.[15], namely der-

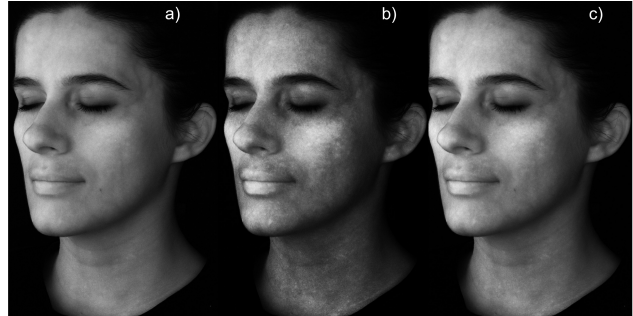


**Figure 9.** Maps of Oxygen Rate within skin computed from the HDR images under red and green illumination in Fig. 2 and the plots in Figure 8. Intermediate results computed from the green and red camera channels respectively (left and center) and final result (right).

mal and epidermal hemoglobin concentrations -  $C_h$  and  $C_{he}$ , represent. Our measurement process provides a direct observation of this concentration without fitting to any specific skin model. Here, we map our blood volume fraction map to the same visualization color coding employed in [15] for the qualitative comparison.



**Figure 10.** Side-by-side comparison of dermal hemoglobin concentration  $C_h$  (left) and epidermal hemoglobin concentration  $C_{he}$  (center) based on the skin appearance model employed by Gitlina et al. [15], with our own blood volume fraction map (right).

We qualitatively compare our blood volume maps computed with the method in the section above with the results of Gevaux et al.[10]. In order to do so we match the visualization of Gevaux with inverse maps of our blood volume maps and brighten our oxygen rate maps. The comparison in Fig. 11 shows we are able to retrieve a blood volume fraction map equivalent to previous work while employing simpler capture hardware. Our signal for oxygen rate is weaker but still enables detection without the use of hyperspectral imaging.

Finally, in Fig. 12, we compare results with the same method but using an RGB LED sphere as the capture setup. Our results (top row) outperform those obtained using the RGB LED sphere setup (bottom row), which utilizes a slightly different RGB camera (Canon 800D) with ostensibly similar spectral sensitivities. We plot the camera sensitivity and the Spectral Distribution of the RGB LED Sphere in Fig. 13.

We find that the fluorescence map extraction and blood volume fraction map accuracy are compromised under the RGB LED sphere illumination, likely due to a shift in the blue LED peak (480nm) compared to LCD panels (450nm), which does not excite elastin fluorescence. Additionally, the reduced gap between the blue and green SPDs in the LED sphere causes mixing of melanin

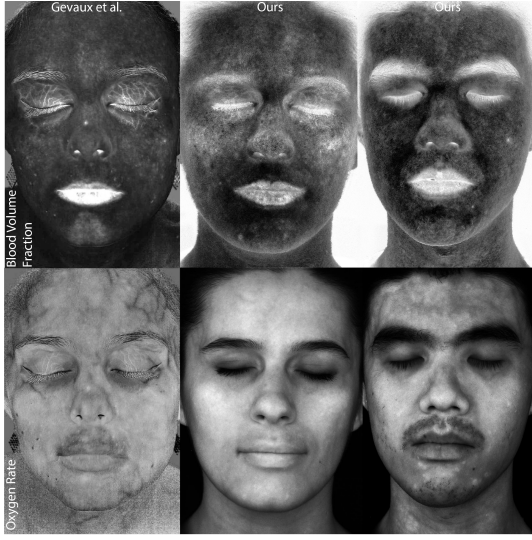


**Figure 11.** Side-by-side qualitative comparison of blood volume fraction (top) and oxygen rate (bottom) between Gevaux et al. [10] (left) and our results (center and right).



**Figure 12.** Comparison of fluorescence, blood volume fraction and oxygen rate obtained with our setup (top), and corresponding results obtained with an RGB LED sphere (bottom).

and blood volume fraction signals. The oxygen rate map measurement with the LED sphere proves to be the most aligned with our results under LCD panel illumination, likely due to similar spectral spacing between the green and red SPDs. This comparison indicates that the RGB SPDs of the LCD panel employed in our setup are more optimal for our measurements than the SPDs of the RGB LEDs of the LED sphere.

## Additional Results

We present additional results respectively in front view and 45° angle view of elastin fluorescence in Fig. 14, blood volume fraction map in Fig. 15 and oxygen rate in Fig. 16. Standard photographs captured under white illumination are provided for all subjects in the supplemental material, along with photographs under our red, green and blue illumination as well as additional results obtained from new subjects.

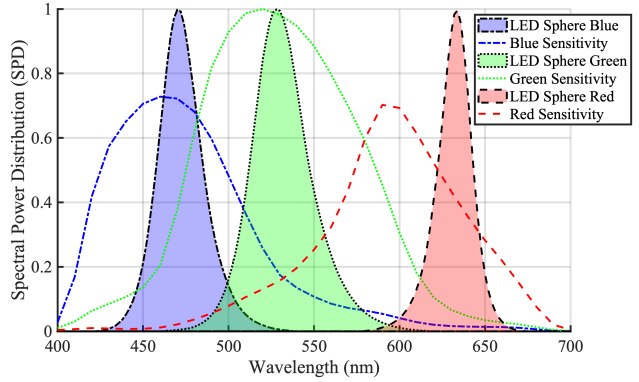


**Figure 13.** The spectral power distributions of the RGB illumination of RGB LED sphere as measured with a spectrometer (Sekonic SpectroMaster C700) and the spectral sensitivity of the RGB cameras (Canon 800D) used for comparison.

As detailed in the sections above, we compute the response of the elastin fluorophore in skin in Fig. 14 for an excitation of 365nm which represents the maximum of excitation for this protein.

Additional blood volume fraction images are presented in Fig. 15. Blood volume fraction shows a consistent trend of female subjects possessing thinner skin layers and displaying more easily networks of capillaries under the skin, particularly on the cheekbones and eyelids, as well as in the lips and ears. The signal varies from individual to individual but tends to be consistent with thinner skin layers which can be due to gender, age or skin conditions [18]. We compute the oxygen rate map, revealing veins marbling the skin at the temples, forehead and cheeks of the subjects.

**Limitations:** The fluorescence signal measured with our capture process is weak due to RGB illumination. Additionally, we cannot measure porphyrin fluorescence which is mostly excited by UV light. Our blood oxygen rate map, compared to hyperspectral imaging, captures areas of strong signal but lacks the precision of results from narrowband illumination and measurement.

## Conclusion

Our study presents an innovative method for assessing skin health by directly measuring elastin fluorescence, blood volume fraction, and oxygen rate using standard RGB imaging with regular LCD panel illumination. This approach allows us to analyze key components of the skin's circulatory system and elastin structure without relying on complex skin models or hyperspectral imaging, making skin optical property assessment more accessible and practical.

The main advantage of our method is its use of readily available, off-the-shelf equipment combined with real-time processing capabilities. This makes it particularly valuable in scenarios requiring rapid decision-making, such as medical imaging applications. Additionally, since skin models rely on optical properties to accurately recreate skin appearance, our method provides a direct and efficient way to measure fluorescence, oxygen rate, and both dermal and epidermal hemoglobin concentrations, thereby enhancing the accuracy of skin-model-based approaches.

However, achieving the comprehensive detail offered by hyperspectral imaging, especially in capturing additional skin components such as melanin, beta-carotene, and collagen fluorescence, remains a challenge. This represents a potential avenue for future research to further enhance the scope and accuracy of skin health assessments.

## Acknowledgments

We thank the volunteer subjects for facial data acquisition. This project has received funding from the European Union's Horizon 2020 research and innovation programme under the Marie Skłodowska-Curie grant agreement No 956585. The work was also partly supported by the following: EPSRC IAA Grant EP/R511547/1 and BBSRC grant BB/X01312X/1.

## References

- [1] Carlos Aliaga, Mengqi Xia, Xao Xie, Adrian Jarabo, Gustav Braun, and Christophe Hery. A hyperspectral space of skin tones for inverse rendering of biophysical skin properties. *Computer Graphics Forum*, 42, 2023.
- [2] Sarah Alotaibi and William A.P. Smith. A biophysical 3d morphable model of face appearance. *Proceedings - 2017 IEEE International Conference on Computer Vision Workshops, ICCVW 2017*, 2018-January:824–832, 2017.
- [3] Leslie Baumann, Eric F Bernstein, Anthony S Weiss, Damien Bates, Shannon Humphrey, Michael Silberberg, and Robert Daniels. Clinical Relevance of Elastin in the Structure and Function of Skin. *Aesthetic Surgery Journal Open Forum*, 3(3):ojab019, 05 2021.
- [4] Symon Cotton, Ela Claridge, and Per Hall. A skin imaging method based on a colour formation model and its application to the diagnosis of pigmented skin lesions. *Proceedings of Medical Image Understanding and Analysis '99*, pages 49–52, 1999.
- [5] David J. Cuccia, Frederic Bevilacqua, Anthony J. Durkin, Frederick R. Ayers, and Bruce J. Tromberg. Quantitation and mapping of tissue optical properties using modulated imaging. *Journal of biomedical optics*, 14:024012, 2009.
- [6] Motonori Doi, Akira Kimachi, Shogo Nishi, Shoji Tominaga, Akira Kimachi, Shogo Nishi, and Shoji Tominaga. Estimation of local skin properties from spectral images and its application to appearance reproduction. *Journal of Imaging Science and Technology*, 60:1–11, 9 2016.
- [7] R Donaldson. Spectrophotometry of fluorescent pigments. *British Journal of Applied Physics*, 5(6):210–214, 1954.
- [8] Craig Donner and Henrik Wann Jensen. A spectral bssrdf for shading human skin. In *Proceedings of the 17th Eurographics Conference on Rendering Techniques, EGSR '06*, page 409–417, Goslar, DEU, 2006. Eurographics Association.
- [9] Craig Donner, Tim Weyrich, Eugene D'Eon, Ravi Ramamoorthi, and Szymon Rusinkiewicz. A layered, heterogeneous reflectance model for acquiring and rendering human skin. *ACM SIGGRAPH Asia 2008 Papers, SIGGRAPH Asia'08*, 2008.
- [10] Lou Gevaux, Cyprien Adnet, Pierre Séroul, Raphael Clerc, Alain Tréneau, Jean Luc Perrot, and Mathieu Hébert. Three-dimensional hyperspectral imaging: a new method for human face acquisition. *Electronic Imaging*, 30(8):152–1–152–1, 2018.
- [11] Lou Gevaux, Jordan Gierschendorf, Juliette Rengot, Marie Cherel, Pierre Séroul, Alex Nkengne, Julie Robic, Alain Tréneau, and Mathieu Hébert. Real-time skin chromophore estimation from hyperspectral images using a neural network. *Skin Research and Technology*, 2020.
- [12] Abhijeet Ghosh, Graham Fyffe, Borom Tunwattanapong, Jay Busch, Xueming Yu, and Paul Debevec. Multiview face capture using polarized spherical gradient illumination. *ACM Transactions on Graphics (TOG)*, 30:1–10, 12 2011.
- [13] Robert Gillies, George Zonios, Rox R. Anderson, and Nikiforos Kollias. Fluorescence excitation spectroscopy provides information about human skin in vivo. *Journal of Investigative Dermatology*, 115, 2000.
- [14] Y. Gitlina, G. C. Guarnera, D. S. Dhillon, J. Hansen, A. Lattas, D. Pai, and A. Ghosh. Practical measurement and reconstruction of spectral skin reflectance. *Computer Graphics Forum*, 39:75–89, 2020.
- [15] Yuliya Gitlina, Daljit Singh J. Dhillon, Jan Hansen, Dinesh K. Pai, and Abhijeet Ghosh. Practical measurement-based spectral rendering of human skin. In *ACM SIGGRAPH 2018 Posters, SIGGRAPH '18*, New York, NY, USA, 2018. Association for Computing Machinery.
- [16] Paulo Gotardo, Jérémie Rivière, Derek Bradley, Abhijeet Ghosh, and Thabo Beeler. Practical dynamic facial appearance modeling and acquisition. *ACM Transactions on Graphics (TOG)*, 12 2018.
- [17] Takanori Igarashi, Ko Nishino, and Shree K. Nayar. The appearance of human skin: A survey. *Foundations and Trends® in Computer Graphics and Vision*, 3:1–95, 7 2007.
- [18] Jose A. Iglesias-Guitian, Carlos Aliaga, Adrian Jarabo, and Diego Gutierrez. A biophysically-based model of the optical properties of skin aging. *Computer Graphics Forum*, 34(2):45–55, 2015.
- [19] Henrik Wann Jensen, Stephen R. Marschner, Marc Levoy, and Pat Hanrahan. A practical model for subsurface light transport. In *Proceedings of the 28th Annual Conference on Computer Graphics and Interactive Techniques, SIGGRAPH '01*, page 511–518, New York, NY, USA, 2001. Association for Computing Machinery.
- [20] Jorge Jimenez, Diego Gutierrez, Timothy Scully, Tim Weyrich, Nuno Barbosa, Craig Donner, Xenxo Alvarez, Teresa Vieira, Paul Matts, and Verónica Orvalho. A practical appearance model for dynamic facial color. *ACM Transactions on Graphics (TOG)*, 29:1–10, 12 2010.
- [21] Oliver Klehm, Fabrice Roussel, Marios Papas, Derek Bradley, Christophe Hery, Bernd Bickel, Wojciech Jarosz, and Thabo Beeler. Recent advances in facial appearance capture. *Computer Graphics Forum*, 34:709–733, 5 2015.

- [22] N. Kollias, R. Gillies, M. Moran, I. E. Kochevar, and R. R. Anderson. Endogenous skin fluorescence includes bands that may serve as quantitative markers of aging and photoaging. *Journal of Investigative Dermatology*, 111, 1998.
- [23] Alexandros Lattas, Yiming Lin, Jayanth Kannan, Ekin Ozturk, Luca Filipi, Giuseppe Claudio Guarnera, Gaurav Chawla, and Abhijeet Ghosh. Practical and scalable desktop-based high-quality facial capture. *European Conference on Computer Vision 2022*, 2022.
- [24] Guolan Lu and Baowei Fei. Medical hyperspectral imaging: a review. *Journal of biomedical optics*, 19:010901, 1 2014.
- [25] Scott Prahl. Optical absorption of hemoglobin.
- [26] Yang Pu, Wubao Wang, Guichen Tang, and Robert R. Alfano. Changes of collagen and nicotinamide adenine dinucleotide in human cancerous and normal prostate tissues studied using native fluorescence spectroscopy with selective excitation wavelength. <https://doi.org/10.1117/1.3463479>, 15:047008, 7 2010.
- [27] Canfield Scientific. Visia skin analysis.
- [28] Pierre Seroul, Mathieu Hébert, Marie Chérel, Romain Vernet, Raphael Clerc, Matthieu Jomier, and Marie Cherel. Model-based skin pigment cartography by high-resolution hyperspectral imaging. *Journal of Electronic Imaging*, 69:48–56, 2016.
- [29] Norimichi Tsumura, Nobutoshi Ojima, Kayoko Sato, Mitsuhiro Shiraishi, Hideto Shimizu, Hirohide Nabeshima, Syuichi Akazaki, Kimihiko Hori, and Yoichi Miyake. Image-based skin color and texture analysis/synthesis by extracting hemoglobin and melanin information in the skin. *ACM Trans. Graph.* 22, 2003.
- [30] Tim Weyrich, Jason Lawrence, Hendrik P.A. Lensch, Szymon Rusinkiewicz, and Todd Zickler. Principles of appearance acquisition and representation. *Foundations and Trends® in Computer Graphics and Vision*, 4:75–191, 2009.
- [31] George Zonios, Julie Bykowski, and Nikiforos Kollias. Skin melanin, hemoglobin, and light scattering properties can be quantitatively assessed in vivo using diffuse reflectance spectroscopy. *The Journal of investigative dermatology*, 117:1452–1457, 2001.

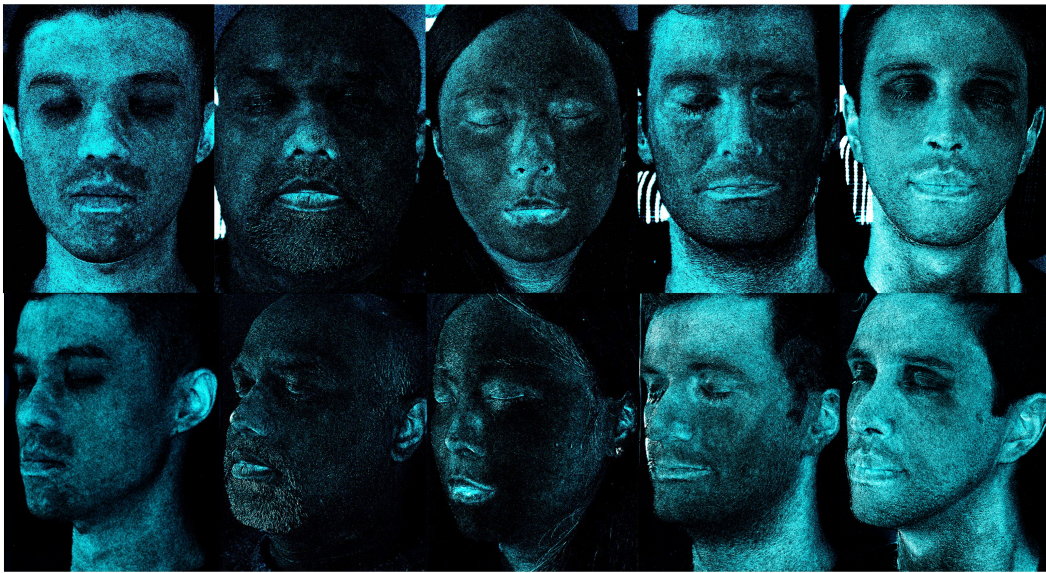


Figure 14. Front View of Elastin Fluorescence Concentration Map



Figure 15. Front View of Blood Volume Fraction Map



Figure 16. Front View of Oxygen Rate Map